



Unravelling the metabolic alterations of liver damage induced by thirdhand smoke

Sònia Torres^{a,b}, Sara Samino^{a,c}, Pere Ràfols^{a,c}, Manuela Martins-Green^d, Xavier Correig^{a,b,c}, Noelia Ramírez^{a,b,c,*}

^a Department of Electronic Engineering, Universitat Rovira i Virgili, Tarragona, Catalonia, Spain

^b Institut d'Investigació Sanitària Pere Virgili, Tarragona, Catalonia, Spain

^c CIBERDEM, Spanish Biomedical Research Centre in Diabetes and Associated Metabolic Disorders, Barcelona, Catalonia, Spain

^d Department of Molecular, Cell and Systems Biology, University of California, Riverside CA 92521, USA

ARTICLE INFO

Handling editor: Shoji Nakayama

Keywords:

Thirdhand smoke
NMR-based metabolomics
LC-based metabolomics
Mass Spectrometry Imaging
Liver damage
NAFLD

ABSTRACT

Background: Thirdhand smoke (THS) is the accumulation of tobacco smoke gases and particles that become embedded in materials. Previous studies concluded that THS exposure induces oxidative stress and hepatic steatosis in liver. Despite the knowledge of the increasing danger of THS exposure, the metabolic disorders caused in liver are still not well defined.

Objectives: The aim of this study is to investigate the metabolic disorders caused by THS exposure in liver of male mice and to evaluate the effects of an antioxidant treatment in the exposed mice.

Methods: We investigated liver from three mice groups: non-exposed mice, exposed to THS in conditions that mimic human exposure and THS-exposed treated with antioxidants. Liver samples were analyzed using a multiplatform untargeted metabolomics approach including nuclear magnetic resonance (¹H NMR), liquid chromatography coupled to high-resolution mass spectrometry (LC-HRMS) and laser desorption/ionization mass spectrometry imaging (MSI), able to map lipids in liver tissues.

Results: Our multiplatform approach allowed the annotation of eighty-eight metabolites altered by THS exposure, including amino acids, nucleotides and several types of lipids. The main dysregulated pathways by THS exposure were D-glutamine and D-glutamate metabolism, glycerophospholipid metabolism and oxidative phosphorylation and glutathione metabolism, being the last two related to oxidative stress. THS-exposed mice also presented higher lipid accumulation and decrease of metabolites involved in the phosphocholine synthesis, as well as choline deficiency, which is related to Non-Alcoholic Fatty Liver Disease and steatohepatitis. Interestingly, the antioxidant treatment of THS-exposed mice reduced the accumulation of some lipids, but could not revert all the metabolic alterations, including some related to the impairment of the mitochondrial function.

Conclusions: THS alters liver function at a molecular level, dysregulating many metabolic pathways. The molecular evidences provided here confirm that THS is a new factor for liver steatosis and provide the basis for future research in this respect.

1. Introduction

Non-Alcoholic Fatty Liver Disease (NAFLD) is becoming the most common chronic liver disorder in the western countries affecting both adults and children. The prevalence of NAFLD in Europe has reached very high levels (20–30%) (ELPA European Liver Patients' Association, 2019) and it is expected to grow across many countries in the years to come. NAFLD comprises different stages starting with non-alcoholic

fatty liver (NAFL) and non-alcoholic steatohepatitis (NASH) which can progress to more severe and irreversible stages of the disease such as fibrosis, cirrhosis and hepatocellular carcinoma (HCC) (Haas et al., 2016). As a result, NAFLD is becoming a leading indication for liver transplantation and cause of hepatocellular carcinoma (Adam et al., 2012; Bertuccio et al., 2017). Due to the importance of the early detection at previous stages by non-invasive techniques, current research focuses on finding reliable biomarkers to predict disease stages

* Corresponding author at: IISPV-URV-CIBERDEM, Av. Paisos Catalans, 26, 43007-Tarragona, Spain.

E-mail address: noelia.ramirez@urv.cat (N. Ramírez).

<https://doi.org/10.1016/j.envint.2020.106242>

Received 12 May 2020; Received in revised form 16 August 2020; Accepted 22 October 2020

Available online 13 November 2020

0160-4120/© 2020 The Author(s).

Published by Elsevier Ltd.

This is an open access article under the CC BY-NC-ND license

(<http://creativecommons.org/licenses/by-nc-nd/4.0/>).

and development (Pirola and Sookoian, 2018). Since NAFLD is seen as a lifestyle condition, it is vital to determine all the risk factors associated with its prevalence. Previous research demonstrated that tobacco consumption is a risk factor in NAFLD development (Akhavan Rezayat et al., 2018; Hamabe et al., 2011; Kim et al., 2018; Pei Yi et al., 2017), and that the exposure to secondhand smoke (SHS) also increases this risk (Liu et al. 2013; Yuan et al. 2009).

Nevertheless, exposure to tobacco smoke toxicants goes beyond SHS exposure. A less studied path of exposure is the so-called thirdhand smoke (THS) that is formed by the accumulation of tobacco smoke toxicants that settle on furniture, fabrics and surfaces in places where SHS was present (Jacob et al., 2017; Matt et al., 2011). These toxicants can also react with atmospheric oxidants to form secondary pollutants that could have increased toxicity (Sleiman et al., 2010), such as tobacco-specific nitrosamines, a leading class of carcinogens that affect humans (IARC International Agency for Research on Cancer, 2007). Recently, several studies have presented undeniable evidences of THS health hazards, including liver damage in *in vitro* and *in vivo* models (Flores et al., 2017, 2016; Hang et al., 2017; Jacob et al., 2017). THS exposure of mice caused abnormal lipid metabolism in liver, enhancing the accumulation of lipids in larger lipid droplets in the hepatocytes with higher concentrations of triglycerides that is induced by oxidative stress. This accumulation of lipids can result in the development of NAFLD (Adhami et al., 2016; Flores et al., 2016; Martins-Green et al., 2014). After four weeks of THS exposure, male mice presented an increase of the liver damage biomarker aspartate aminotransferase (AST), and from two months there were signs of molecular damage induced by oxidative stress, including an increase of hydrogen peroxide (H₂O₂) and superoxide dismutase (SOD) (Adhami et al., 2017). The decrease of the oxidative stress with antioxidants ameliorated the THS-induced damage (Adhami et al., 2016; Chen et al., 2018; Flores et al., 2016). Moreover, acute and chronic exposure to THS of human liver cancer cells (HepG2) significantly increased DNA strand breaks (Hang et al., 2013). In view of these results, THS exposure could be a new risk factor for the development of hepatic steatosis. Nevertheless, the extent of the molecular alterations in liver induced by THS exposure remains to be fully elucidated.

Here we present a novel approach for the comprehensive molecular characterization of THS-induced liver damage based on multiplatform untargeted metabolomics of liver samples from male mice exposed to THS in conditions that mimic exposure of humans in the homes of smokers. In order to determine if antioxidants could completely revert THS-induced molecular damage, some of the THS-exposed mice were treated with antioxidants. Untargeted metabolomics is a powerful tool that allows the simultaneous determination of hundreds of metabolites in biological samples and, therefore, is key to elucidate metabolic changes and disorders (Siuzdak et al., 2012). We have performed untargeted analysis of aqueous and lipidic liver extracts using two complementary analytical platforms to cover a wider range of metabolites: proton nuclear magnetic resonance (¹H NMR) and liquid chromatography coupled to high resolution mass spectrometry (LC-HRMS). Furthermore, we have also explored the spatial distribution of lipids in the liver samples by acquiring mass spectrometry images of liver sections using an innovative methodology based on sputtered gold nanolayers and laser desorption ionization mass spectrometry (LDI-MS). To our knowledge, this is the first study that assess the potential of a multiplatform metabolomics approach to unravel the molecular alterations of THS-induced liver damage.

2. Materials and methods

2.1. Animal models

Animal models were developed at the Molecular, Cell and Systems Biology Department at the University of California Riverside. Male C57BL/6 mice model and THS exposure methodology was described by

Martins-Green et al. (Flores et al., 2016; Martins-Green et al., 2014). Briefly, different household materials were exposed to secondhand smoke (SHS) from a smoking machine. Total particulate matter was $30 \pm 5 \mu\text{g}/\text{m}^3$, which is within the range of fine particles detected in smokers' homes (Semple et al., 2015). For this study, male mice were randomly divided into three experimental groups (5 mice for each group): control (CTRL), which was never exposed to THS; THS-exposed (THS) that were placed in the exposed cages from weaning (three weeks of age) to 24 weeks; and a third group of mice exposed to THS and then treated intraperitoneally with the antioxidants alpha-tocopherol (alpha-toc) and N-acetylcysteine (NAC) for 20 weeks while the mice still continued to be exposed to THS (THS-AO). THS and THS-AO groups were never exposed to SHS, and all groups were fed a standard chow diet (percent calories: 58% carbohydrates, 28.5% protein, and 13.5% fat). In order to assure the reliability of the THS exposure model, we measured the concentration of 4-(methylnitrosoamino)-1-(3-pyridyl)-1-butanol (NNAL) in the urine of mice that is the main metabolite of the tobacco-specific nitrosamine 4-(methylnitrosoamino)-1-(3-pyridyl)-1-butanone (NNK), a well-accepted biomarker of exposure to tobacco toxicants (Torres et al., 2018). Median urine concentration of NNAL of THS-exposed mice was 35 pg mL^{-1} , 20% less than NNAL levels in urine of SHS-exposed infants/toddlers, confirming the suitability of our THS exposure model (Martins-Green et al., 2014).

Animal experimental protocols were approved by the University of California, Riverside, Institutional Animal Care and Use Committee (IACUC). Mice were euthanized with Carbon dioxide (CO₂) inhalation which is the most common method of euthanasia used by NIH for mice. The levels and time for CO₂ exposure were approved by the University of California, Riverside IACUC, death was induced quickly and without pain. Liver samples were snap frozen and kept at -80°C until analysis.

2.2. Untargeted metabolomics analysis

To cover a wider range of metabolites, we performed untargeted metabolomics analysis using two complementary analytical platforms: ¹H NMR and LC-HRMS.

For ¹H NMR analysis, five liver samples of each experimental group were lyophilized overnight and mechanically pulverized. Twenty mg of dried liver powder of each sample were extracted twice with 1.5 and 0.5 mL of a precooled acetonitrile–water mixture (1:1) by vigorous vortexing for 30 s, followed by the extraction of the hydrophilic metabolites in an ultrasound ice bath for 5 min. After centrifugation at 15000 rpm for 15 min at 4°C , the combined supernatants from both extractions were dried and redissolved with 700 μL of phosphate buffer (Na₂HPO₄/NaH₂PO₄, 0.2 M, in D₂O) containing 0.7 mM NaN₃ and 2.3 mM of 3-(trimethylsilyl)propionic-2,2,3,3-d₄ acid sodium salt (TSP-d₄) as chemical shift reference. For the extraction of the lipophilic metabolites, the pellets from the previous extraction were mixed with 1 mL of chloroform: methanol (2:1) and extracted as commented above. Lipidic extracts were dried under a gentle N₂ stream and reconstituted with 700 μL of a mixture of CDCl₃, CD₃OD and D₂O (64:32:4) containing 1.18 mM tetramethylsilane (TMS). Following centrifugation, 650 μL of each extract was transferred into a 5 mm NMR tube for ¹H NMR analysis. Liver extracts (aqueous and lipidic) were analyzed using a Bruker ADVANCE III 600 instrument (Bruker Biospin GmbH, Rheinstetten, Germany). ¹H NMR spectra were recorded at 310 K on a spectrometer operating at a proton frequency of 600.20 MHz. For the aqueous extracts, one-dimensional ¹H pulse experiments were carried out using a nuclear Overhauser effect spectroscopy (NOESY)-presaturation sequence to suppress the residual water peak at around 4.7 ppm for aqueous extracts. The relaxation delay between scans was set to 5 s. Spectral width was 16 ppm and a total of 256 transients were collected for each spectrum. In the case of lipophilic extracts, a 90° pulse with presaturation sequence (zgpr) was used. Spectral width was 18.6 ppm and a total of 128 transients were collected for each spectrum.

The acquired one dimensional (1D) ¹H NMR spectra were phased,

baseline-corrected and referenced to glucose signal (5.23 ppm) for the aqueous extracts and to TMS signal for the lipidic extracts with TopSpin from Bruker. After baseline correction, peaks in the 1D spectra were integrated using the AMIX 3.8 software package (Bruker). Metabolites were annotated with level 1 confidence following the Rank and Assign Confidence to Metabolites (RANCM) proposed by Joesten et al. (Joesten and Kennedy, 2019), by comparing their chemical shifts with those obtained from standard compounds from Chenomx NMR Suite Professional database (Chenomx Inc., Edmonton, Canada), BBIoref AMIX database (Bruker), Human metabolome database, version 3.0 (Wishart et al., 2012) and previous bibliography (Vinaixa et al., 2010). Relative concentrations derived from both aqueous and lipidic extracts were arranged together in one single data matrix, which was used as the input matrix to perform the statistical analysis using RStudio (version 3.3.2, Boston, MA). Student's *t*-test FDR-adjusted *p*-value < 0.05 and absolute fold change (FC) ≥ 1.1 were considered to indicate statistically significant differences between the experimental groups.

Based on previous literature, aliquots of the extracts prepared for the ^1H NMR analysis were directly analyzed by LC-MS (Beltran et al., 2012). Three μL of the aqueous extracts were injected into a 1290 Infinity LC System coupled to a 6230 ESI-QTOF mass spectrometer (both from Agilent Technologies, Palo Alto, CA, USA), using an ACQUITY UHPLC HSS T3 C_{18} column (2.1 mm \times 150 mm, 1.8 μm) from Waters (Eschborn, Germany), kept at 30 $^\circ\text{C}$ during the whole analysis. The mobile phases consisted of ultrapure water containing 0.1% formic acid (A) and acetonitrile with 0.1% formic acid (B) at a flow rate of 0.45 mL min^{-1} . The gradient elution program was as follows: 100% A for 2 min, 100% A to 100% B from 2 to 9 min, 100% B from 9 to 10 min, and 100% A from 10 to 12 min.

Fifty μL of the lipidic extracts used for the ^1H NMR analysis were evaporated to dryness and reconstituted with 100 μL of methanol:toluene (9:1). Three μL of these reconstituted extracts were injected into the same LC-MS instrument. Separation was performed as described by Pi et al. (Pi et al., 2016) using an ACQUITY UHPLC BEH C18 column (2.1 mm \times 150 mm, 1.7 μm ; Waters), and mobile phases: A: acetonitrile: water (60:40) with 10 mM of ammonium formate and B: isopropanol: acetonitrile (90:10) with 10 mM of ammonium formate.

For both analyses, the mass spectrometer operated in positive electrospray ionization (ESI+) mode in the following conditions: gas temperature, 150 $^\circ\text{C}$; drying gas, 11 L min^{-1} ; nebulizer, 35 psi; fragmentor, 120 V; and skimmer, 65 V. The instrument was set to acquire over the *m/z* range 100–1000 for the aqueous extracts and 50–1200 for the lipidic ones, at an acquisition rate of 3 spectra s^{-1} . To assure the quality of the analysis, the extracts were injected in randomized order and quality control (QC) samples (prepared by pooling equal volumes of all aqueous and lipidic extracts, respectively) were injected every 5 samples.

LC-HRMS data was processed using the XCMS software, version 2.9.2 (Smith et al., 2006) to detect and align features. Those features with intensity lower than 5,000 spectral counts and variation lower than those found in the QC samples were discarded. Features found in at least 80% of samples were used for univariate statistical analysis. Those filtered features that were statistically different between the studied groups (*p*-value < 0.05, Student's *t*-test, FDR corrected, and FC > 2) were putatively annotated by searching against the HMDB, version 3.0 (Wishart et al., 2012) within 5 ppm mass error threshold. The putatively annotated features with a candidate for the $[\text{M} + \text{H}]^+$ adduct and relevant biological interest were confirmed by Tandem MS (MS/MS) performed in targeted mode, acquiring over the *m/z* range 50–1000, with a narrow isolation width (~ 1.3 *m/z*) and a fixed collision energy of 20 V. Annotation was carried out by comparing the obtained experimental mass fragmentation spectra with those experimental spectra from open access databases (HMDB, METLIN (Smith et al., 2005) and LipidMaps (Fahy et al., 2007), with a level 2 identification confidence, in accordance with Schymanski et al. (coincidence of exact mass of the precursor ion (MS) and fragmentation pattern (MS^2)) (Schymanski et al., 2014). Two-way hierarchical clustering was performed using MetaboAnalyst

software (Chong et al., 2019).

Data obtained from the ^1H NMR and LC-HRMS analysis are accessible at the Zenodo Open Access Repository (<https://zenodo.org>), under DOI: <https://doi.org/10.5281/zenodo.3986136>.

2.3. Pathway analysis

The statistically relevant metabolites annotated by untargeted metabolomics in the liver extracts (including both, aqueous and lipidic extracts) were used to determine the metabolic pathways altered by THS exposure. Pathway enrichment analysis was performed using MBROLE 2.0 (Chagoyen and Pazos, 2011), selecting *mus musculus* as organism-based background. Only pathways over enriched with a *p*-value < 0.05 (FDR-corrected) were considered for the biological interpretation of the results. Fold enrichment (FE) of each altered metabolic pathway was calculated using the following formula $\text{FE} = (m/n)/(M/N)$ (Huang et al., 2009), being *m*: the metabolites annotated in our study that belong to a specific metabolic pathway; *n*: the total number of metabolites annotated in our study; *M*: the total number of metabolites in a pathway; and *N*: all the metabolites of mice (*mus musculus*) reported in the database.

2.4. Mass spectrometry imaging

Mass spectrometry images were acquired using a matrix-free laser desorption/ionization methodology developed in our research group that is based on the deposition of gold sputtered nanolayers on tissue sections (Ràfols et al., 2018). Briefly, liver tissues were sectioned at -20 $^\circ\text{C}$ into 10 μm thick sections using a Leica CM-1950 cryostat (Leica Biosystems Nussloch GmbH) and mounted on indium-tin oxide-coated (ITO) glass slides by directly placing the glass slide at ambient temperature onto the section. Gold nanolayers were deposited onto the 10 μm tissue sections using a sputtering system ATC Orion 8-HV (AJA International, N. Scituate, MA, USA). Histological images were acquired by examining serial liver sections stained with Oil Red O (ORO) using standard protocols. MSI images were acquired using a MALDI TOF/TOF UltrafleXtreme instrument with SmartBeam II Nd:YAG/355 nm laser from Bruker Daltonics (Massachusetts, USA) and a raster size of 20 μm .

LDI-MSI spectra data handling, alignment, calibration, peak picking (selecting peaks with signal-to-noise ratio > 5) and peak binning were carried out using the in-house developed R package rMSIproc (Ràfols et al., 2020). MS images reconstruction and visual inspection was performed with rMSI package (Ràfols et al., 2017), which allows the reconstruction of the ion intensity images and the calculation of average spectra of regions of interest.

3. Results

3.1. Untargeted metabolomics results

Combining untargeted metabolomics analysis by ^1H NMR and LC-HRMS, we were able to annotate 108 relevant metabolites in the aqueous (52) and lipidic (56) liver extracts. Supplementary Material, Section S1 and Section S2 present detailed information about the selection of relevant features and metabolite annotation by both analytical platforms.

Table 1 shows the complete list of statistically different metabolites annotated in the aqueous extracts, including their *p*-values (FDR corrected) and FC for the different comparisons between the experimental groups (CTRL vs. THS, THS vs. THS-AO) and the analytical platform that allowed the annotation. As it can be seen in Table 1, the annotated metabolites in the aqueous extracts included amino acids, coenzymes, nucleotides, peptides and organic acids, among others. Adenosine monophosphate (AMP) and glutamine were annotated by both analytical platforms, giving consistent results in both cases. For these two metabolites we present the results obtained by LC-HRMS, because this

Table 1

Metabolites annotated in the aqueous extracts that were statistically relevant between THS-exposed and non-exposed liver samples (CTRL vs. THS), between THS-exposed mice and those exposed to THS and treated with antioxidants (THS vs. THS-AO). For each metabolite, the FDR corrected p-value and fold change (FC) of each comparison and the determination technique is also indicated. (Abbreviations: NAD: Nicotinamide adenine nucleotide; NADP: Nicotinamide adenine dinucleotide phosphate; AMP: Adenosine monophosphate; ADP: Adenosine diphosphate).

Metabolite	CTRL vs. THS		THS vs. THS-AO		Technique
	p-value (FDR)	FC	p-value (FDR)	FC	
Serotonin	2.87 × 10 ⁻⁰³	12.4	2.90 × 10 ⁻⁰²	-13.1	LC-MS/MS
Octanoylcarnitine	1.65 × 10 ⁻⁰²	11.6			LC-MS/MS
Decanoylcarnitine	4.49 × 10 ⁻⁰²	6.9			LC-MS/MS
N-α-Acetyl-arginine	5.13 × 10 ⁻⁰³	6.8			LC-MS/MS
N6-Acetyl-lysine	9.20 × 10 ⁻⁰³	5.1			LC-MS/MS
NAD	7.67 × 10 ⁻⁰³	4.7			LC-MS/MS
Leucyl-Isoleucine	1.51 × 10 ⁻⁰²	3.8			LC-MS/MS
Adenosine diphosphate ribose	6.82 × 10 ⁻⁰³	3.5			LC-MS/MS
Hexanoyl carnitine	2.22 × 10 ⁻⁰²	2.9			LC-MS/MS
Nα-Acetyl-glutamine	2.62 × 10 ⁻⁰²	2.9			LC-MS/MS
AMP	8.83 × 10 ⁻⁰³	2.4	3.63 × 10 ⁻⁰³	-1.3	LC-MS/MS
Isobutyrylglycine	1.09 × 10 ⁻⁰²	2.3			LC-MS/MS
5-Methylcytidine	3.24 × 10 ⁻⁰²	2.2	3.24 × 10 ⁻⁰²	2.2	LC-MS/MS
Xanthine	5.92 × 10 ⁻⁰⁴	2.2			LC-MS/MS
Adenine	8.81 × 10 ⁻⁰⁴	2.1			LC-MS/MS
γ-Glutamylglycine	7.32 × 10 ⁻⁰⁴	1.8			LC-MS/MS
Argininic Acid	1.01 × 10 ⁻⁰²	1.6			LC-MS/MS
Glutamine	2.21 × 10 ⁻⁰³	1.6			LC-MS/MS
Pyrrolidone carboxylic acid	2.19 × 10 ⁻⁰³	1.6			LC-MS/MS
NADP	1.80 × 10 ⁻⁰²	1.5	1.06 × 10 ⁻⁰²	-1.4	¹ H NMR
Xanthosine	3.67 × 10 ⁻⁰³	1.5			LC-MS/MS
Glycine	1.80 × 10 ⁻⁰²	1.1			¹ H NMR
Glutathione	1.96 × 10 ⁻⁰³	-1.2			¹ H NMR
3-Hydroxybutyrate	8.51 × 10 ⁻⁰³	-1.3			¹ H NMR
Isoleucine	4.30 × 10 ⁻⁰³	-1.3	2.97 × 10 ⁻⁰²	1.4	¹ H NMR
Phenylalanine	1.02 × 10 ⁻⁰²	-1.3	1.77 × 10 ⁻⁰²	-1.3	¹ H NMR
Succinate	1.59 × 10 ⁻⁰²	-1.3	3.41 × 10 ⁻⁰⁵	1.5	¹ H NMR
Valine	1.96 × 10 ⁻⁰³	-1.3			¹ H NMR
Acetate	1.02 × 10 ⁻⁰³	-1.4	2.27 × 10 ⁻⁰²	1.3	¹ H NMR
Creatine	4.30 × 10 ⁻⁰³	-1.4	2.68 × 10 ⁻⁰²	1.3	¹ H NMR
Tyrosine	3.70 × 10 ⁻⁰³	-1.4			¹ H NMR
3-Methylxanthine	7.50 × 10 ⁻⁰³	-1.5	1.46 × 10 ⁻⁰²	1.3	¹ H NMR

Table 1 (continued)

Metabolite	CTRL vs. THS		THS vs. THS-AO		Technique
	p-value (FDR)	FC	p-value (FDR)	FC	
Niacinamide	9.12 × 10 ⁻⁰³	-1.6	4.45 × 10 ⁻⁰²	1.4	¹ H NMR
Glutamate	6.48 × 10 ⁻⁰⁴	-1.7	7.69 × 10 ⁻⁰⁵	1.4	¹ H NMR
Uridine	1.67 × 10 ⁻⁰³	-1.7	5.67 × 10 ⁻⁰⁶	1.9	¹ H NMR
Betaine	4.44 × 10 ⁻⁰⁴	-1.8	2.19 × 10 ⁻⁰²	1.4	¹ H NMR
Choline	8.65 × 10 ⁻⁰⁴	-2	3.97 × 10 ⁻⁰³	1.3	¹ H NMR
Pantothenic Acid	4.66 × 10 ⁻⁰²	-2			LC-MS/MS
Inosine	1.09 × 10 ⁻⁰²	-2.1	6.52 × 10 ⁻⁰⁴	1.7	¹ H NMR
Tryptophan	1.94 × 10 ⁻⁰³	-2.2			LC-MS/MS
1,7-Dimethylguanosine	2.05 × 10 ⁻⁰²	-2.5			LC-MS/MS
Glutamyl-Lysine	3.15 × 10 ⁻⁰³	-2.6			LC-MS/MS
O-phosphocholine	4.44 × 10 ⁻⁰⁴	-2.9	2.41 × 10 ⁻⁰²	1.4	¹ H NMR
Cytidine	6.25 × 10 ⁻⁰³	-3			LC-MS/MS
Glycogen	3.36 × 10 ⁻⁰²	-3			LC-MS/MS
Cytosine	9.54 × 10 ⁻⁰³	-3.1			LC-MS/MS
5- Glutamyl-alanine	6.48 × 10 ⁻⁰³	-3.6			LC-MS/MS
Aminoadipic acid	4.89 × 10 ⁻⁰³	-9.1			LC-MS/MS
ADP	2.82 × 10 ⁻⁰³	-12.9			LC-MS/MS
Glucose			4.33 × 10 ⁻⁰²	1.2	¹ H NMR
Lactate			3.07 × 10 ⁻⁰²	-1.1	¹ H NMR
Taurine			2.99 × 10 ⁻⁰²	1.4	¹ H NMR

analytical platform provided the lower p values. Exposure to THS resulted in the alteration of forty-nine aqueous metabolites (Table 1, “CTRL vs. THS” columns), evidencing the impact of THS exposure in liver at the molecular level. Treatment with antioxidants was able to regulate the concentrations of twenty of the aqueous metabolites (Table 1, “THS vs. THS-AO” columns). As an example, serotonin, which is recognized to affect various liver diseases (Lesurtel et al., 2012), was the most upregulated metabolite annotated in THS mice livers (FC_(CTRL vs. THS) = 12.4, but the levels of serotonin decreased under the antioxidant treatment of THS exposed mice (FC_(THS vs. THS-AO) = -13.1). Nevertheless, we found that the antioxidant treatment was not able to revert all the molecular alterations induced by THS exposure. This was the case, for instance, of the levels of some acylcarnitines (i.e. Octanoylcarnitine, Decanoylcarnitine, Hexanoylcarnitine), that were increased by THS exposure and remained increased with the antioxidant treatment. Antioxidant treatment was also not able to revert the decrease of the nucleotides cytidine and cytosine, as well as, tryptophan and adenosine diphosphate (ADP), among others.

The untargeted analysis of the lipidic extracts lead to the annotation of fifty-six metabolites statistically different between the studied groups. ¹H NMR analysis also allowed the annotation of five differential groups of lipids (monounsaturated fatty acids (MUFAs), polyunsaturated fatty acids (PUFAs), total and free cholesterol and triglycerides (TG)). The complete list of these metabolites can be found at Table 2, including the analytical platform that allowed their annotation, as well as, the p values and FC of each statistical comparison between groups. As it can be seen

Table 2

Metabolites annotated in the lipidic extracts that were statistically relevant between THS-exposed and non-exposed liver samples (CTRL vs. THS) and between THS-exposed mice and those exposed to THS and treated with antioxidants (THS vs. THS-AO). For each metabolite, the FDR corrected p-value and fold change (FC) of each comparison and the determination technique is also indicated. (Abbreviations: TG: triglyceride, PC: phosphocholine, LysoPC: Lyso-phosphocholine, DHA: Docosahexaenoic acid, SM: sphingomyelin).

Metabolites	CTRL vs. THS		THS vs. THS-AO		Technique
	p-value FDR	Fold Change	p-value FDR	Fold Change	
TG (52:6)	4.70 × 10 ⁻⁰³	9.2	2.90 × 10 ⁻⁰²	-3.5	LC-MS/MS
PC (42:6)	4.60 × 10 ⁻⁰⁴	6.9			LC-MS/MS
TG (54:7)	5.06 × 10 ⁻⁰³	5	7.11 × 10 ⁻⁰³	-2.1	LC-MS/MS
TG (50:4)	1.62 × 10 ⁻⁰²	4.9			LC-MS/MS
TG (32:2)	3.81 × 10 ⁻⁰³	4.5	1.65 × 10 ⁻⁰²	-2.7	LC-MS/MS
TG (50:2)	3.17 × 10 ⁻⁰³	3.4			LC-MS/MS
TG (54:8)	1.80 × 10 ⁻⁰²	3.4	4.46 × 10 ⁻⁰³	-3.6	LC-MS/MS
TG (54:6)	7.37 × 10 ⁻⁰³	3.3			LC-MS/MS
PE (36:6)	3.32 × 10 ⁻⁰⁴	3.3			LC-MS/MS
TG (50:2)	1.19 × 10 ⁻⁰³	3.2	2.21 × 10 ⁻⁰⁴	-2.6	LC-MS/MS
TG (56:6)	3.44 × 10 ⁻⁰³	3.1			LC-MS/MS
TG (52:5)	8.81 × 10 ⁻⁰³	2.9			LC-MS/MS
PC (32:1)	8.08 × 10 ⁻⁰⁴	2.9			LC-MS/MS
LysoPC (16:1)	7.32 × 10 ⁻⁰³	2.9			LC-MS/MS
PC (36:6)	1.96 × 10 ⁻⁰³	2.9			LC-MS/MS
Triglycerides	5.80 × 10 ⁻⁰³	2.7	2.09 × 10 ⁻⁰²	-1.8	¹ H NMR
TG (51:3)	5.43 × 10 ⁻⁰³	2.7			LC-MS/MS
LysoPC (18:1)	1.60 × 10 ⁻⁰²	2.7			LC-MS/MS
PC (17:1)	1.15 × 10 ⁻⁰²	2.7			LC-MS/MS
PC (36:4)	1.07 × 10 ⁻⁰³	2.5			LC-MS/MS
TG (51:1)	2.94 × 10 ⁻⁰³	2.4			LC-MS/MS
PC (34:3)	4.47 × 10 ⁻⁰⁴	2.3			LC-MS/MS
TG (49:2)	4.31 × 10 ⁻⁰³	2.3			LC-MS/MS
TG (48:1)	1.47 × 10 ⁻⁰³	2.3			LC-MS/MS
TG (54:2)	1.49 × 10 ⁻⁰³	2.2			LC-MS/MS
PC (38:7)	1.22 × 10 ⁻⁰⁴	2.1			LC-MS/MS
Oleic acid	7.56 × 10 ⁻⁰³	1.7			¹ H NMR
Linoleic acid	1.25 × 10 ⁻⁰²	1.3			¹ H NMR
DHA	8.03 × 10 ⁻⁰³	1.2	1.87 × 10 ⁻⁰²	1.2	¹ H NMR
Monounsaturated Fatty Acids	5.80 × 10 ⁻⁰³	1.2			¹ H NMR
Polyunsaturated Fatty Acids	4.37 × 10 ⁻⁰²	1.1	2.09 × 10 ⁻⁰²	1.2	¹ H NMR
Free Cholesterol	8.77 × 10 ⁻⁰³	-1.2	1.16 × 10 ⁻⁰³	1.5	¹ H NMR
Total Cholesterol		-1.3		1.5	¹ H NMR

Table 2 (continued)

Metabolites	CTRL vs. THS		THS vs. THS-AO		Technique
	p-value FDR	Fold Change	p-value FDR	Fold Change	
	5.80 × 10 ⁻⁰³		2.68 × 10 ⁻⁰³		
Coenzyme Q9	1.06 × 10 ⁻⁰³	-2			LC-MS/MS
PC (36:0)	5.93 × 10 ⁻⁰⁴	-2.3	1.37 × 10 ⁻⁰²	3.2	LC-MS/MS
SM (42:2)	3.27 × 10 ⁻⁰⁴	-2.3			LC-MS/MS
SM (36:1)	2.45 × 10 ⁻⁰⁴	-2.3			LC-MS/MS
PC (34:0)	9.55 × 10 ⁻⁰³	-3.7	5.67 × 10 ⁻⁰³	2.1	LC-MS/MS
PC (34:1)	2.53 × 10 ⁻⁰²	-3.8			LC-MS/MS
Esterified Cholesterol			3.58 × 10 ⁻⁰⁴	2.8	¹ H NMR
PC (35:2)			1.56 × 10 ⁻⁰³	2	LC-MS/MS
PC (36:5)			3.21 × 10 ⁻⁰³	-2.5	LC-MS/MS
PC (38:1)			2.99 × 10 ⁻⁰²	2.3	LC-MS/MS
PC (39:4)			9.29 × 10 ⁻⁰⁴	-2.5	LC-MS/MS
PC (40:4)			6.20 × 10 ⁻⁰⁴	-3.3	LC-MS/MS
PC(41:7)			1.97 × 10 ⁻⁰⁴	-7.4	LC-MS/MS
Phosphatidylcholine			7.48 × 10 ⁻⁰³	1.3	¹ H NMR
Phosphatidylethanolamine			6.49 × 10 ⁻⁰³	1.2	¹ H NMR
Phosphatidylserine			2.67 × 10 ⁻⁰⁴	2.7	¹ H NMR
SM (16:1)			1.96 × 10 ⁻⁰³	2.9	LC-MS/MS
Sphingomyelin			8.51 × 10 ⁻⁰⁴	2.4	¹ H NMR
TG (36:2)			1.55 × 10 ⁻⁰²	-2	LC-MS/MS
TG(48:2)*			1.12 × 10 ⁻⁰³	-3.7	LC-MS/MS
TG (51:2)			3.14 × 10 ⁻⁰³	-2.3	LC-MS/MS
TG (56:2)			1.12 × 10 ⁻⁰²	-4.8	LC-MS/MS
TG (56:3)			9.58 × 10 ⁻⁰³	-2.3	LC-MS/MS

in Table 2, thirty-nine of the metabolites annotated in the lipidic extracts were altered because of THS exposure (Table 2, "CTRL vs. THS" columns). In accordance with previous works, THS exposure increased lipid concentrations, being triglycerides the lipid family that presented higher concentrations in the THS liver samples (Flores et al., 2016; Martins-Green et al., 2014). The comprehensive untargeted metabolomics approach presented here allowed the annotation of 21 different triglycerides, as well as other types of lipids such as oleic, linoleic and docosahexaenoic acids (DHA), MUFAs, PUFAs, seven unsaturated phosphocholines (PC) and two lysophosphocholines (lysoPC) that were increased by THS exposure. Conversely, we found that some saturated phosphocholines (PC) (i.e. PC(36:0), PC(34:0)), sphingomyelins (SM) (i.e. SM(42:2), SM (36:1)), Coenzyme Q9 and free and total cholesterol decreased by THS exposure. Interestingly, the concentration of esterified cholesterol was not affected by THS exposure. In agreement with previous studies (Flores et al., 2016), the antioxidant treatment of THS exposed mice, decreased the total concentrations of lipids in liver, including the total concentration of triglycerides, DHA, and sphingomyelin. Nevertheless, the antioxidant treatment could not regulate the THS induced alterations of many of the altered lipids including

coenzyme Q9, MUFAs, oleic and linoleic acids and different kind of TGs, PCs and SMs. It also intensified the increase of PUFAs.

The aqueous and lipidic annotated metabolites significantly different in the CTRL vs. THS and the THS vs. THS-AO comparisons were subject to hierarchical clustering, to illustrate the variation of concentrations in the three studied groups. The obtained heatmap of the relative concentrations is represented in Fig. 1. For the metabolites represented here, CTRL and THS-AO groups clustered together. This figure also shows the clustered metabolites, such as the represented TGs, NADP and serotonin (increased by THS exposure and reverted by the antioxidant treatment), acetate, total and free cholesterol, isoleucine, uridine and succinate (decreased by THS exposure, but increased by the antioxidant treatment), or phenylalanine and AMP, whose deficiency caused by THS

exposure was more pronounced by antioxidants.

To further illustrate the metabolic differences between the studied groups commented during this section, [Supplementary material, Figure S1](#) shows the average ^1H NMR spectra of the aqueous extracts and the individual spectra of some metabolites ([Figure S1a](#)). The differences between the 3 studied groups can also be seen in the chromatographic peaks of the acquired LC-HRMS chromatograms shown in [Figure S1b](#). Analogously, [Supplementary material, Figure S2](#) shows the acquired ^1H NMR spectra ([Figure S2a](#)) and LC-MS chromatograms ([Figure S2b](#)) of the liver lipidic extracts. The detailed signals of some annotated lipids clearly show how the antioxidant treatment decrease the concentration of some types of lipids, such as triglycerides. However, it also shows that the concentrations of other lipids, such as sphingomyelins, were higher

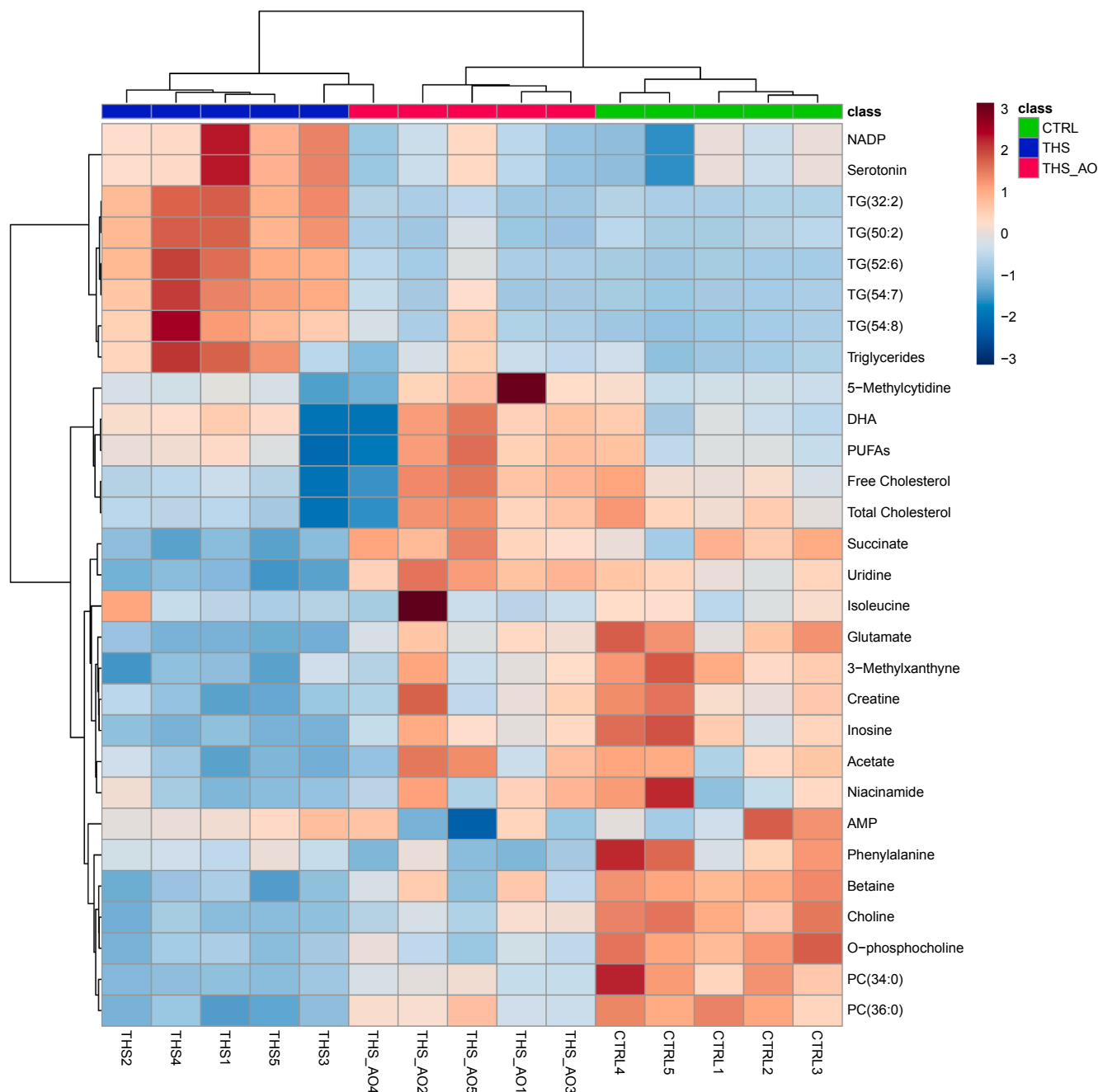


Fig. 1. Heatmap representing two-way hierarchical cluster analysis of the statistically relevant metabolites in both, aqueous and lipidic extracts, for the exposure to THS (CTRL vs. THS) and for the effect of the antioxidant intake of THS-exposed mice (THS vs. THS-AO). Clustering of samples is shown on the top axis and clustering of features on the left axis. Colors represent median relative intensity of each studied group.

in liver samples of THS-AO mice than in those from CTRL and THS mice, indicating that the concentrations of these types of lipids were more influenced by the antioxidant treatment rather than THS-exposure. The combined effects of THS exposure and the antioxidant treatment against the non-treated group are presented at the [Supplementary material](#), Section S3 and Table S2.

The findings presented so far suggest, that although the antioxidant treatment would be able to balance some of the metabolic alterations in liver induced by THS, the possible side effects associated to the combination of THS exposure and antioxidants must be object of further study.

3.2. Spatial distribution of lipids

The histological images of liver sections representative of CTRL, THS and THS-AO stained with oil red O (ORO) at two magnifications ($\times 40$ and $\times 100$ zoom) are shown in [Fig. 2a-f](#). As it could be seen in these figures, lipid droplet sizes were between 1.2 and 2.0 μm in CTRL liver sections, from 2.5 to 3.9 μm in THS and between 1.6 and 3.0 μm in THS-AO liver sections ([Fig. 2d-f](#)). In accordance with previous studies ([Martins-Green et al., 2014](#)), lipid droplets were more abundant and larger in the THS-exposed mice ([Fig. 2b & 2e](#)). Furthermore, these images show that the antioxidant treatment reduced the number and size of lipid droplets regarding the THS group, but not at the levels of the CTRL group. The average LDI-MS spectra in the m/z region 750–1000 Da (corresponding to the majority of lipids) are represented in [Fig. 2g-i](#). In agreement with the histological images, average MS signals of THS-exposed liver sections ([Fig. 2h](#)) were higher than the MS signals of the lipids of CTRL and THS-AO liver samples (up to 6-fold higher than those in the CTRL liver), thus confirming the lipidomic results obtained by untargeted metabolomics. Similarly, MS signals of THS-AO liver sections ([Fig. 2i](#)) were lower than those for THS, but higher than those in the control group (up to 2-fold higher).

MS images of liver sections were analyzed to determine the spatial distribution of the lipids annotated by LC-HRMS that were statistically

relevant between the experimental groups. [Fig. 3](#) shows the spatial distribution of four selected ions (m/z 758.47, m/z 800.51, m/z 873.69 and m/z 899.70, ([Fig. 3a, 3b, 3c](#) and [3d](#), respectively) that were annotated as PE(36:6), PC(36:6), TG(52:6) and TG(54:7) by LC-MS/MS. These lipids were found in the MSI spectra in the form of their corresponding $[M+Na]^+$ adduct within a mass error up to 14 ppm, in agreement with previous observations ([Ràfols et al. 2018](#)). These figures represent the relative abundance of the selected ions in a color scale (showed on the right of the figure), where red represents the zones with higher ion signals and dark blue the ones with lower intensities. As seen in these figures, the relative intensities of these four ions were higher in THS-exposed liver, thus confirming the results obtained by LC-MS/MS. Images also show that the different lipid classes represented here (PE, PC and TG) were similarly distributed in the THS-exposed liver forming comparable images. Since the spatial resolution of the MS images was between 10 and 20 μm , these images cannot draw individual lipid droplets, but areas with higher density of them are represented as red dots. From these images it could be derived that in THS-exposed liver, PE(36:6) and PC(36:6) might be part of the PC layer that forms lipid droplets and that TG (52:6), TG (54:7) and TG (52:6) might be in the core of the lipids droplets, usually formed by TG and stearyl esters (SE) ([Bartz et al., 2007](#)). [Fig. 3](#) also confirms that the treatment with antioxidants drastically reduces the TG accumulation induced by THS exposure, but cannot completely revert the accumulation of other kind of lipids, such as PE(36:6) or PC(36:6).

3.3. Effects of THS exposure in liver metabolism

Pathway enrichment analysis of the relevant metabolites altered in THS-exposed mice revealed that the exposure to THS significantly dysregulated twenty-one metabolic pathways (p-value (FDR corrected) < 0.05) vs. non-exposed mice. [Fig. 4a](#) represents these dysregulated pathways, their p-value and fold enrichment (FE). The most affected metabolic pathways were purine, glutathione, D-glutamine and D-

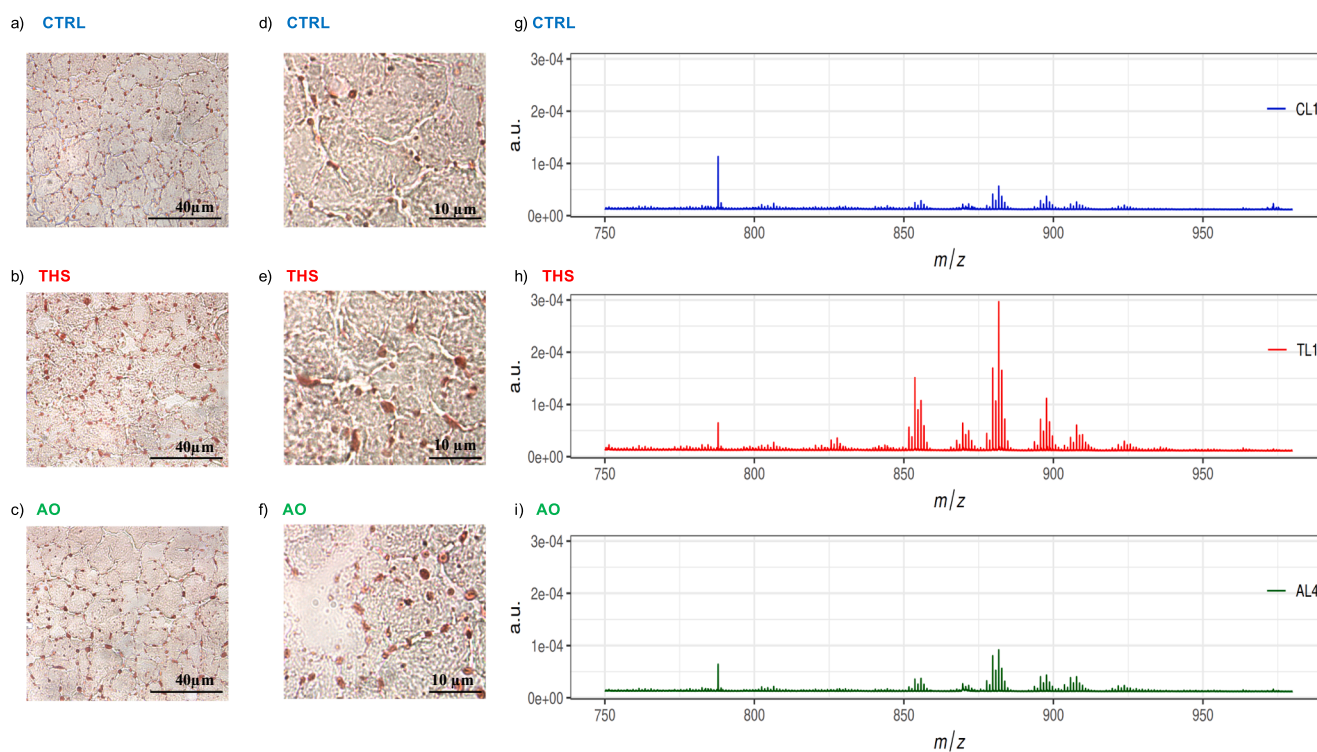


Fig. 2. (A-F) Oil red O stained sections (10 μm of thickness) of liver from CTRL, THS and THS-AO mice, at zooms $\times 40$ (A-C) and $\times 100$ (D-F). (G-I) Average LDI-MSI mass spectra in the lipid range area (m/z 750–1000) of consecutive liver slices, the y-axis represents relative intensity in arbitrary units (a.u.). (For interpretation of the references to color in this figure legend, the reader is referred to the web version of this article.)

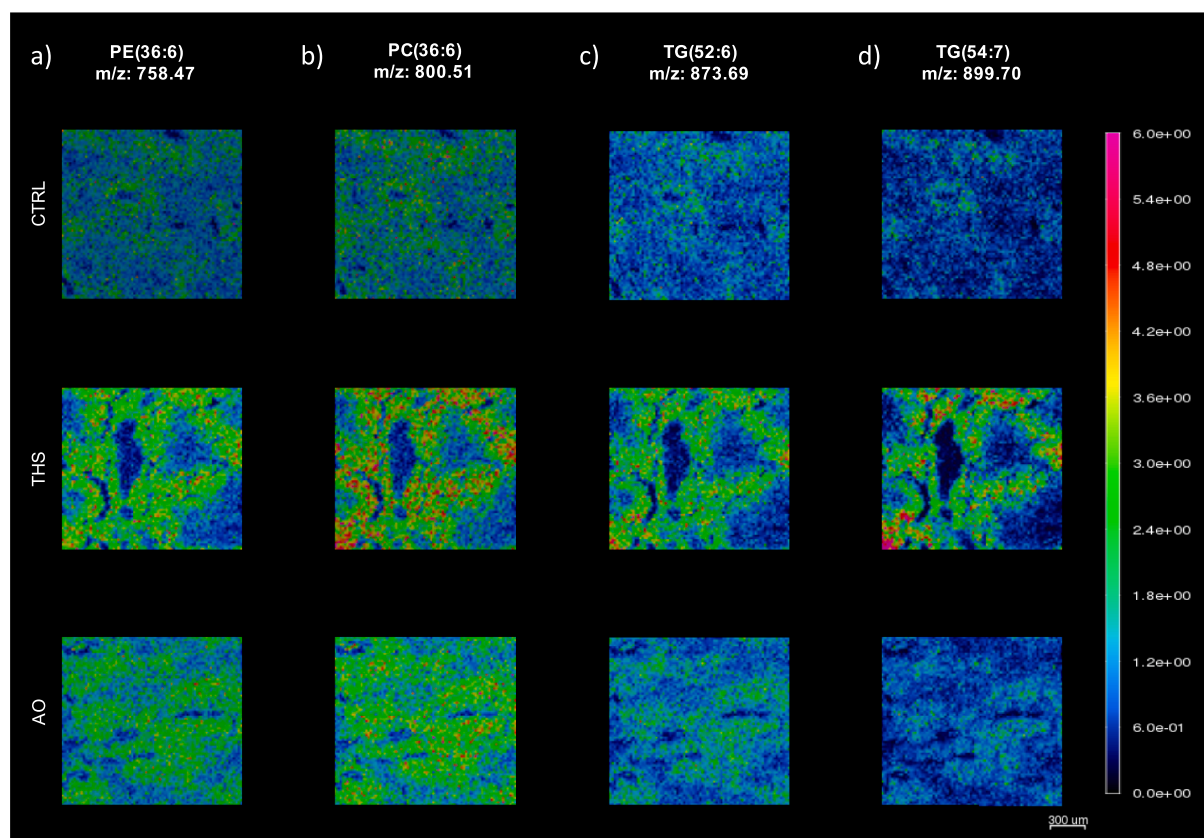


Fig. 3. LDI-MS images of mice liver samples acquired at pixel size of 20 μm . Figures A to D plots the relative abundance of four lipids (758.47 Da, 800.51 Da, 873.69 Da and 899.70 Da, respectively), annotated as the $[\text{M}+\text{Na}]^+$ adducts of (A) PE (36:6), (B) PC(36:6), (C) TG(52:6) and (D) TG(54:7).

glutamate, glycerophospholipid, glycine, serine and threonine, and oxidative phosphorylation metabolisms. Fig. 4c maps the annotated dysregulated metabolites involved in the most altered pathways by THS exposure. D-glutamine and D-glutamate metabolism, oxidative phosphorylation, glutathione and glycerophospholipid metabolism were the metabolic pathways that presented higher FE and, therefore, that have a higher proportion of dysregulated metabolites.

Pathway enrichment between THS and THS-AO groups showed twelve dysregulated metabolic pathways (see Fig. 4b). As seen in this graphic, the most altered pathways because of the antioxidant treatment were glycolysis and gluconeogenesis, glucose-alanine cycle, glycine, serine and threonine and taurine and hypotaurine metabolisms. We can also observe that the antioxidant treatment could only influence five of the metabolic pathways altered by THS exposure (glutathione; glycerophospholipid; glycine, serine and threonine; alanine, aspartate and glutamate; and nicotinate and nicotinamide metabolisms), suggesting that the antioxidant treatment was not able to balance sixteen of the metabolic pathways altered by THS exposure. The metabolic pathways not reverted by antioxidants, included pathways related to lipid regulation, such as phospholipid biosynthesis, oxidative phosphorylation and carnitine synthesis metabolisms and also purine, D-glutamine and D-glutamate and phenylalanine, tyrosine and tryptophan metabolisms.

4. Discussion

Hepatic triglyceride accumulation in liver samples of THS-exposed mice clearly confirmed that THS causes abnormal lipid metabolism known as NAFLD, as it has been previously suggested (Martins-Green et al., 2014). NASH liver characterizes for oxidative stress and lipid accumulation, among others (Rein-Fischboeck et al., 2018). The oxidative stress suffered in liver of THS-exposed mice was demonstrated in previous studies that observed higher superoxide dismutase (SOD)

activity and, as a result, increased levels of H_2O_2 and reactive oxygen species (ROS) (Adhami et al., 2017; Chen et al., 2018; Flores et al., 2016). Flores et al., also found that there was no significant increase in catalase or GPx activity, in consequence H_2O_2 was not properly processed and the levels of reactive oxygen species (ROS) remained high in the liver. They also found that $\text{NADP}^+/\text{NADPH}$ ratio in mice liver, which is an indicator of the cell reducing potential because GPx activity is coupled to the reduction of NADPH to NADP^+ , was decreased significantly because of THS exposure, showing that the reduction potential of these animals was decreased and might result in their inability to reduce the oxidative stress levels induced by the THS toxins. The increase of oxidative stress was in accordance with the increased levels of aspartate aminotransferase (AST) activity found in THS-exposed mice. (Flores et al., 2016).

Our multiplatform untargeted metabolomic approach allowed the annotation of eighty-eight metabolites altered by THS exposure, reporting for the first time some hepatic metabolic alterations caused by THS. At a metabolic level, glutamate and glutathione deficiency found in liver of THS-exposed mice could be linked to increased liver oxidative stress (Wu et al., 2004). Dysregulation of glutathione metabolism induced by THS exposure, agrees with previous findings in reproductive male cells (Hang et al., 2017). Lipidomic results also confirmed the increased oxidative stress in THS-exposed liver, corroborated, for example, by the higher levels of some lysophosphatidylcholines (LPCs) (Pyttel et al., 2012), PUFAs and DHA that are linked to higher risks of lipid peroxidation (Reis and Spickett, 2012).

Our findings also suggest impairment on the hepatic mitochondrial function including decreased levels of AMP and increased levels of some acylcarnitines in the THS-exposed liver samples (Hara et al., 2013; Koves et al., 2008). Besides, THS-exposed mice presented decreased levels of Coenzyme Q9, which plays an important role in mitochondrial energy and serves as a potent endogenous antioxidant.

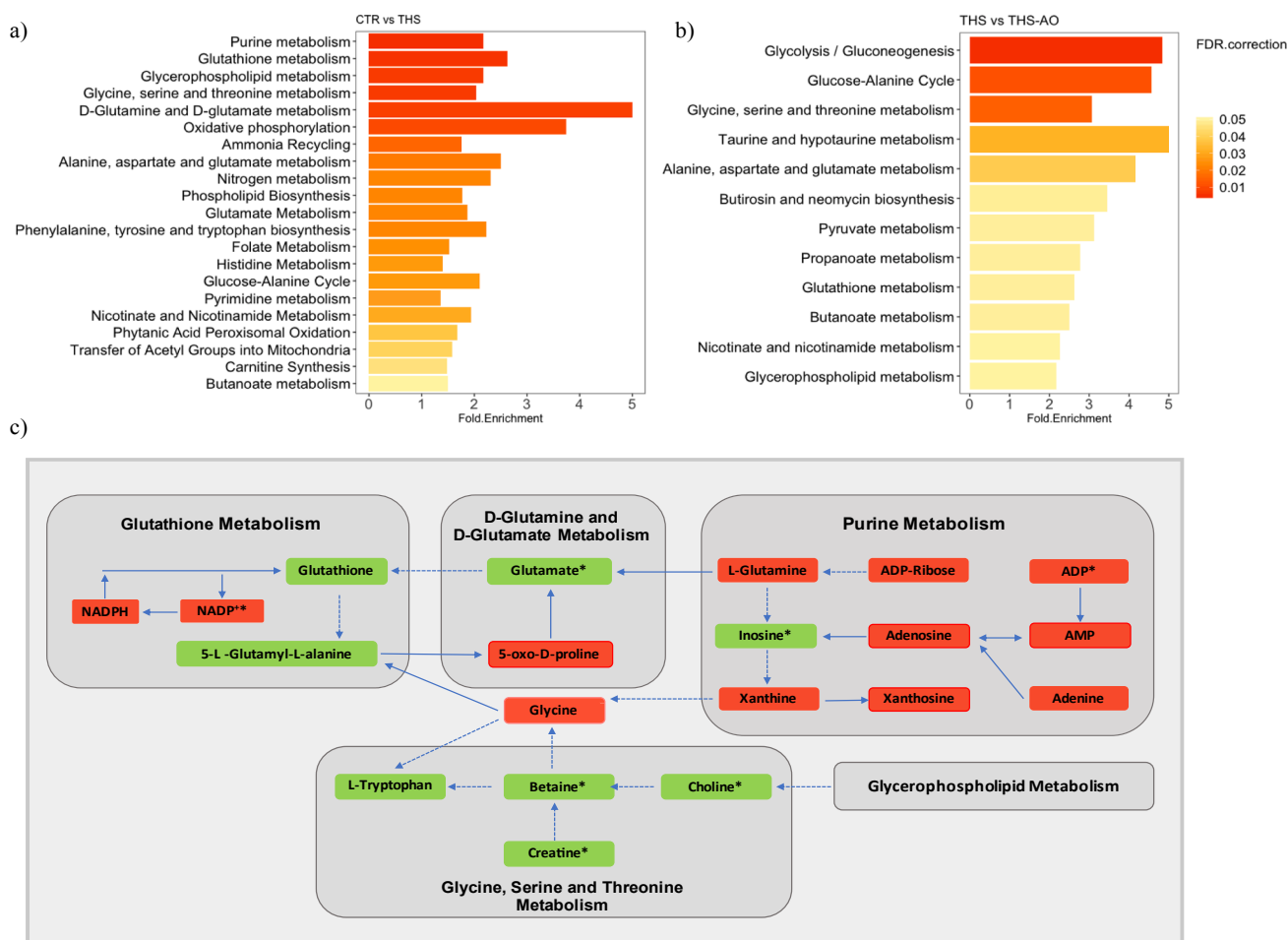


Fig. 4. (A) Metabolic pathways significantly dysregulated due to THS exposure (CTRL vs. THS) arranged from lowest to higher p value (FDR-adjusted $p < 0.05$). Color degradation represents the p-value obtained from the enrichment analysis in MBROLE 2.0 software, and bar length the fold enrichment score. (B) Dysregulated pathways between THS-exposed and THS-exposed treated with antioxidants mice (THS vs. THS-AO). (C) Representation of the altered metabolites included in the metabolic pathways most altered by THS exposure. Up regulated and down regulated metabolites in THS-exposed liver samples are indicated in red and green, respectively. Asterisks indicate those metabolites balanced by the antioxidant treatment. Continuous lines express direct relation between metabolites and dashed lines that there are intermediate metabolites not shown in the figure. (For interpretation of the references to color in this figure legend, the reader is referred to the web version of this article.)

We also found metabolic markers of NAFL and NASH in the THS-exposed group. For instance, the increased levels of hepatic acylcarnitines and linoleic acid found in the THS group were in agreement with previous findings in human liver samples at the stage of NASH (Lake et al., 2015). Acylcarnitines are considered potential biomarkers for liver disease (Flanagan et al., 2010) since they are a key factor regulating the balance of intracellular sugar and lipid metabolism (Li et al., 2019). In addition, several studies have demonstrated the link of acylcarnitines with the development of insulin resistance and type I and type II diabetes (Koves et al., 2008) (Sun et al., 2016). Specifically, decanoylcarnitine and hexanoylcarnitine, which were increased in THS-exposed liver samples, have been significantly associated with diabetes (Sun et al., 2016), increased body fat and waist to hip ratio (Mai et al., 2013). We have also found that all the annotated metabolites related to phosphatidylcholine synthesis including choline, betaine, phosphocholine, PCs and some sphingomyelins (SMs) were decrease in liver samples of the THS group, in agreement with reduced total hepatic phosphatidylcholine (PC) content associated to NAFL and NASH (Jacobs et al., 2013; Rein-Fischboeck et al., 2018). Choline deficiency has an important role in NAFLD, not only in the deposition of triacylglycerol in liver and reduced phospholipid synthesis (Sherriff et al., 2016; Michel et al., 2006), but also in the expression of genes involved in cell proliferation, differentiation and apoptosis, liver dysfunction (Michel et al.,

2006) and cancer (Kwee et al., 2017).

The altered fatty acid profile found in THS exposed liver samples was in accordance with the profile of smokers' plasma developed by Müller et al. (Müller et al., 2014) where the metabolomics analysis revealed that MUFA and oleic acid significantly increased in smokers. The same study also concluded that PC mostly containing MUFA were up regulated in smokers' samples and that saturated PC were down regulated. Our results also show this trend, as the annotated saturated PCs (PC (36:0) and PC (34:0)) were decreased in THS-exposed mice and phosphocholines containing mono and polyunsaturated fatty acids (e.g. PC (32:1), (36:6), (17:1), (36:4), (34:3) and (38:7)) were upregulated in liver of THS-exposed mice. Furthermore, our MS images showed that the lipids forming lipid droplets were unsaturated species consistently with previous observations in yeast cells by Grillitsch et al. (2011). The same authors also observed a higher accumulation of TGs in lipid droplets when cells were grown in oleic acid. Therefore, the increased levels of oleic acid of THS-exposed mice might also be related to the increase of triglycerides and unsaturated lipids in lipid droplets of the THS group.

Considering that previous studies found that oxidative stress might be responsible for most of the THS induced dysregulations in liver, a treatment with antioxidant should be able to mitigate the effects induced by this exposure. In fact, Flores et al. found that mice treated with antioxidants presented H_2O_2 levels similar to non-exposed mice

and significantly lower than THS-exposed ones, and higher GPx activity (Flores et al., 2016). The results of our metabolomics study revealed that although the antioxidant treatment mitigate some of the reported metabolic alterations caused by THS exposure, it was not able to completely revert all of them. This was the case, for instance of glutamate, which is essential in the rate-limiting step of the of glutathione biosynthesis (Franklin et al., 2009). We found that glutamate levels decreased because of THS exposure and, although it increased under the antioxidant treatment, did not returned to the levels found in the control group. Moreover, decreases of glutathione (key in the pathogenesis of liver disease), ADP, Coenzyme Q9 and choline were also not reverted by antioxidants. Further, although antioxidant treatment was able to reduce lipid droplets and generally decrease the accumulation of triglycerides, it could not decrease some lipid levels such as PUFAs, DHA and some carnitines, neither the dysregulation of the carnitine synthesis metabolism found in THS exposed mice, and the health consequences associated to these lipids dysregulations.

Besides, the THS-AO group presented increased levels of glucose and unbalanced glycolysis and gluconeogenesis metabolism. This metabolic pathway was only altered in the THS vs. THS-AO comparison suggesting that a treatment with antioxidants affects this pathway more than THS exposure. Accordingly, we have found that the antioxidant treatment increased glucose levels. This result agrees with increased glucose levels in fasting blood glucose of THS-AO mice (Adhami et al., 2016), suggesting that the combined effect of THS exposure with antioxidants may imbalance other metabolic pathways not specifically altered by THS toxicants.

The results presented here, indicate that THS exposure affects liver metabolism in a complex way and could be the basis of further research to elucidate the molecular mechanisms underlying the toxic effects of THS exposure in liver.

5. Conclusions

The exposure to THS toxicants caused metabolic disorders in liver of exposed mice, producing the dysregulation of dozens of metabolites and several metabolic pathways. Our untargeted metabolomics multiplatform approach has been revealed as a powerful tool for the annotation of metabolites that can potentially serve as biomarkers of early biological effects involved in THS exposure. We annotated 88 significant metabolites included in 21 metabolic pathways dysregulated because of THS exposure. The exposure to THS toxicants significantly increased the accumulation of triglycerides in liver, altered the fatty acid, phosphocholine and acylcarnitine profiles, increasing the size and occurrence of lipid droplets. These findings support the relationship between THS exposure and NAFLD risk, in addition to the possible evolution to NASH due to the acute oxidative stress suffered in liver. The results found in THS exposed livers treated with antioxidants confirmed that oxidative stress is one of the major causes of THS-induced liver disease. The intake of antioxidants balanced some metabolite alterations induced by THS, but it was unable to revert all the molecular damage, including key metabolites in mitochondrial function and the hepatic metabolism of phospholipids and carnitines. Our study demonstrates the merit of multiple analytical platform-based metabolomics as a valuable approach for the annotation of biomarkers involved in NAFLD as well as dysregulated metabolites involved in THS exposure.

CRedit authorship contribution statement

Sonia Torres: Methodology, Formal analysis, Data curation, Investigation, Writing - original draft, Visualization. **Sara Samino:** Methodology, Formal analysis, Data curation. **Pere Ràfols:** Methodology, Software. **Manuela Martins-Green:** Conceptualization, Methodology, Writing - review & editing. **Xavier Correig:** Writing - review & editing, Supervision. **Noelia Ramírez:** Conceptualization, Supervision, Writing - review & editing, Project administration, Funding acquisition.

Declaration of Competing Interest

None.

Acknowledgements

This research was funded by the European Union's Horizon 2020 research and innovation programme under the Marie Skłodowska-Curie grant agreement No. 660034; the Spanish Ministry of Science & Innovation through N.R.'s Juan de la Cierva Incorporación grant No. (IJCI-2015-23158) and TEC2015-69076-P project; N.R.'s Miguel Servet contract (CP19/00060) from Instituto de Salud Carlos III, co-financed by Fondo Europeo de Desarrollo Regional (FEDER), Unión Europea, "Una manera de hacer Europa"; and the Tobacco-Related Disease Research Program (TRDRP) of the University of California under projects 22RT-0121 and 23DT-0103.

Appendix A. Supplementary material

Supplementary data to this article can be found online at <https://doi.org/10.1016/j.envint.2020.106242>.

References

- Adam, R., Karam, V., Delvart, V., O'Grady, J., Mirza, D., Klempnauer, J., Castaing, D., Neuhaus, P., Jamieson, N., Salizzoni, M., Pollard, S., Lerut, J., Paul, A., Garcia-Valdecasas, J.C., Rodríguez, F.S.J., Burroughs, A., 2012. Evolution of indications and results of liver transplantation in Europe. A report from the European Liver Transplant Registry (ELTR). *J. Hepatol.* 57, 675–688. <https://doi.org/10.1016/j.jhep.2012.04.015>.
- Adhami, N., Chen, Y., Martins-Green, M., 2017. Biomarkers of disease can be detected in mice as early as 4 weeks after initiation of exposure to third-hand smoke levels equivalent to those found in homes of smokers. *Clin. Sci.* 131, 2409–2426. <https://doi.org/10.1042/CS20171053>.
- Adhami, N., Starck, S.R., Flores, C., Green, M.M., 2016. A health threat to bystanders living in the homes of smokers: How smoke toxins deposited on surfaces can cause insulin resistance. *PLoS One* 11, 1–20. <https://doi.org/10.1371/journal.pone.0149510>.
- Akhavan Rezaei, A., Dadgar Moghadam, M., Ghasemi Nour, M., Shirazinia, M., Ghodsi, H., Rouhbakhsh Zahmatkesh, M.R., Tavakolizadeh Noghabi, M., Hoseini, B., Akhavan Rezaei, K., 2018. Association between smoking and non-alcoholic fatty liver disease: A systematic review and meta-analysis. *SAGE Open Med.* <https://doi.org/10.1177/2050312117745223>.
- Bartz, R., Zehmer, J.K., Zhu, M., Chen, Y., Serrero, G., Zhao, Y., Liu, P., 2007. Dynamic Activity of Lipid Droplets: Protein Phosphorylation and GTP-Mediated Protein Translocation. <https://doi.org/10.1021/pr070158j>.
- Beltran, A., Suarez, M., Rodríguez, M.A., Vinaixa, M., Samino, S., Arola, L., Correig, X., Yanes, O., 2012. Assessment of compatibility between extraction methods for NMR- and LC/MS-based metabolomics. *Anal. Chem.* <https://doi.org/10.1021/ac3005567>.
- Bertuccio, P., Turati, F., Carioli, G., Rodríguez, T., La Vecchia, C., Malvezzi, M., Negri, E., 2017. Global trends and predictions in hepatocellular carcinoma mortality. *J. Hepatol.* 67, 302–309. <https://doi.org/10.1016/j.jhep.2017.03.011>.
- Chagoyen, M., Pazos, F., 2011. MBRole: enrichment analysis of metabolomic data. *Bioinformatics* 27, 730–731. <https://doi.org/10.1093/bioinformatics/btr001>.
- Chen, Y., Adhami, N., Martins-Green, M., 2018. Biological markers of harm can be detected in mice exposed for two months to low doses of Third Hand Smoke under conditions that mimic human exposure. *Food Chem. Toxicol.* 122, 95–103. <https://doi.org/10.1016/j.fct.2018.09.048>.
- Chong, J., Wishart, D.S., Xia, J., 2019. Using MetaboAnalyst 4.0 for Comprehensive and Integrative Metabolomics Data Analysis. *Curr. Protoc. Bioinforma.* <https://doi.org/10.1002/cpbi.86>.
- ELPA (European Liver Patients' Association). Annual Report 2017 [Available: <https://elpa.eu/wp-content/uploads/2019/06/Annual-Report-2017.pdf>] [accessed: 14 August 2019].
- Fahy, E., Sud, M., Cotter, D., Subramaniam, S., 2007. LIPID MAPS online tools for lipid research. *Nucl. Acids Res.* 35, W606–W612. <https://doi.org/10.1093/nar/gkm324>.
- Flanagan, J.L., Simmons, P.A., Vehige, J., Willcox, M.D., Garrett, Q., 2010. Role of carnitine in disease. *Nutr. Metab.* 7, 1–14. <https://doi.org/10.1186/1743-7075-7-30>.
- Flores, C., Adhami, N., Green, M.M., 2016. THS Toxins Induce Hepatic Steatosis by Altering Oxidative Stress and SIRT1 Levels. *J. Clin. Toxicol.* 06, 1–11. <https://doi.org/10.4172/2161-0495.1000318>.
- Flores, C., Adhami, N., Martins Green, M., 2017. The Role of Fatty Acid Metabolism and Apolipoproteins in Ths-Induced Hepatic Steatosis in Mice. *Ferment. Technol.* 07 <https://doi.org/10.4172/2167-7972.1000359>.
- Franklin, C.C., Backos, D.S., Mohar, I., White, C.C., Forman, H.J., Kavanagh, T.J., 2009. Structure, function, and post-translational regulation of the catalytic and modifier subunits of glutamate cysteine ligase. *Mol. Aspects Med.* 30, 86–98. <https://doi.org/10.1016/j.mam.2008.08.009>.

- Grillitsch, K., Connerth, M., Köfeler, H., Arrey, T.N., Rietschel, B., Wagner, B., Karas, M., Daum, G., 2011. Lipid particles/droplets of the yeast *Saccharomyces cerevisiae* revisited: Lipidome meets Proteome. *Biochim Biophys. Acta - Mol. Cell Biol. Lipids* 1811, 1165–1176. <https://doi.org/10.1016/j.bbalip.2011.07.015>.
- Haas, J.T., Franque, S., Staels, B., 2016. Pathophysiology and Mechanisms of Nonalcoholic Fatty Liver Disease. *Annu. Rev. Physiol.* 78, 181–205. <https://doi.org/10.1146/annurev-physiol-021115-105331>.
- Hamabe, A., Uto, H., Imamura, Y., Kusano, K., Mawatari, S., Kumagai, K., Kure, T., Tamai, T., Moriuchi, A., Sakiyama, T., Oketani, M., Ido, A., Tsubouchi, H., 2011. Impact of cigarette smoking on onset of nonalcoholic fatty liver disease over a 10-year period. *J. Gastroenterol.* 46, 769–778. <https://doi.org/10.1007/s00535-011-0376-z>.
- Hang, B., Sarker, A.H., Havel, C., Saha, S., Hazra, T.K., Schick, S., Jacob, P., Rehan, V.K., Chenna, A., Sharan, D., Sleiman, M., Destailats, H., Gundel, L.A., 2013. Thirdhand smoke causes DNA damage in human cells. *Mutagenesis* 28, 381–391. <https://doi.org/10.1093/mutage/get013>.
- Hang, B., Wang, P., Zhao, Y., Sarker, A., Chenna, A., Xia, Y., Snijders, A.M., Mao, J.H., 2017. Adverse health effects of thirdhand smoke: From cell to animal models. *Int. J. Mol. Sci.* 18 <https://doi.org/10.3390/ijms18050932>.
- Hara, H., Araya, J., Ito, S., Kobayashi, K., Takasaka, N., Yoshii, Y., Wakui, H., Kojima, J., Shimizu, K., Numata, T., Kawaiishi, M., Kamiya, N., Odaka, M., Morikawa, T., Kaneko, Y., Nakayama, K., Kuwano, K., 2013. Mitochondrial fragmentation in cigarette smoke-induced bronchial epithelial cell senescence. *Am. J. Physiol. - Lung Cell. Mol. Physiol.* 305 <https://doi.org/10.1152/ajplung.00146.2013>.
- Huang, D.W., Sherman, B.T., Lempicki, R.A., 2009. Systematic and integrative analysis of large gene lists using DAVID bioinformatics resources. *Nat. Protoc.* <https://doi.org/10.1038/nprot.2008.211>.
- IARC (International Agency for Research on Cancer). IARC monographs on the evaluation of the carcinogenic risk to humans - smokeless tobacco and some tobacco-specific N-nitrosamines, vol.89. Lyon, France: WHO; 2007 [Available: <http://monographs.iarc.fr/ENG/Monographs/vol89/> [accessed: 12 August 2020]].
- Jacob, P., Benowitz, N.L., Destailats, H., Gundel, L., Hang, B., Martins-Green, M., Matt, G.E., Quintana, P.J.E., Samet, J.M., Schick, S.F., Talbot, P., Aquilina, N.J., Hovell, M.F., Mao, J.H., Whitehead, T.P., 2017. Thirdhand smoke: New evidence, challenges, and future directions. *Chem. Res. Toxicol.* 30, 270–294. <https://doi.org/10.1021/acs.chemrestox.6b00343>.
- Jacobs, R.L., van der Veen, J.N., Vance, D.E., 2013. Finding the balance: The role of S-adenosylmethionine and phosphatidylcholine metabolism in development of nonalcoholic fatty liver disease. *Hepatology* 58, 1207–1209. <https://doi.org/10.1002/hep.26499>.
- Joesten, W.C., Kennedy, M.A., 2019. RANCM: a new ranking scheme for assigning confidence levels to metabolite assignments in NMR-based metabolomics studies. *Metabolomics* 15. <https://doi.org/10.1007/s11306-018-1465-2>.
- Kim, N.H., Jung, Y.S., Hong, H.P., Park, J.H., Kim, H.J., Park, D. II, Cho, Y.K., Sohn, C. II, Jeon, W.K., Kim, B.I., 2018. Association between cotinine-verified smoking status and risk of nonalcoholic fatty liver disease. *Liver Int.* 1–8 <https://doi.org/10.1111/liv.13701>.
- Koves, T.R., Ussher, J.R., Noland, R.C., Slentz, D., Mosedale, M., Ilkayeva, O., Bain, J., Stevens, R., Dyck, J.R.B., Newgard, C.B., Lopaschuk, G.D., Muoio, D.M., 2008. Mitochondrial Overload and Incomplete Fatty Acid Oxidation Contribute to Skeletal Muscle Insulin Resistance. *Cell Metab.* 7, 45–56. <https://doi.org/10.1016/j.cmet.2007.10.013>.
- Kwee, S.A., Sato, M.M., Kuang, Y., Franke, A., Custer, L., Miyazaki, K., Wong, L.L., 2017. [18F]Fluorocholine PET/CT Imaging of Liver Cancer: Radiopathologic Correlation with Tissue Phospholipid Profiling. *Mol. Imaging Biol.* 19, 446–455. <https://doi.org/10.1007/s11307-016-1020-3>.
- Lake, A.D., Novak, P., Shipkova, P., Aranibar, N., Robertson, D.G., Reily, M.D., Lehman-Mckeeman, L.D., Vaillancourt, R.R., Cherrington, N.J., 2015. Branched chain amino acid metabolism profiles in progressive human nonalcoholic fatty liver disease. *Amino Acids* 47, 603–615. <https://doi.org/10.1007/s00726-014-1894-9>.
- Lesurtel, M., Soll, C., Humar, B., Clavien, P.A., 2012. Serotonin: A double-edged sword for the liver? *Surgeon* 10, 107–113. <https://doi.org/10.1016/j.surge.2011.11.002>.
- Li, S., Gao, D., Jiang, Y., 2019. Function, detection and alteration of acylcarnitine metabolism in hepatocellular carcinoma. *Metabolites* 9. <https://doi.org/10.3390/metabo9020036>.
- Liu, Y., Dai, M., Bi, Y., Xu, M., Xu, Y., Li, M., Wang, T., Huang, F., Xu, B., Zhang, J., Li, X., Wang, W., Ning, G., 2013. Active Smoking, Passive Smoking, and Risk of Nonalcoholic Fatty Liver Disease (NAFLD): A Population-Based Study in China. *J. Epidemiol.* 23, 115–121. <https://doi.org/10.2188/jea.JE20120067>.
- Mai, M., Tönjes, A., Kovacs, P., Stumvoll, M., Fiedler, G.M., Leichtle, A.B., 2013. Serum levels of acylcarnitines are altered in prediabetic conditions. *PLoS One* 8. <https://doi.org/10.1371/journal.pone.0082459>.
- Martins-Green, M., Adhami, N., Frankos, M., Valdez, M., Goodwin, B., Lyubovitsky, J., Dhall, S., Garcia, M., Egiebor, I., Martínez, B., Green, H.W., Havel, C., Yu, L., Liles, S., Matt, G., Destailats, H., Sleiman, M., Gundel, L.A., Benowitz, N., Jacob, P., Hovell, M., Winickoff, J.P., Curras-Collazo, M., 2014. Cigarette smoke toxins deposited on surfaces: Implications for human health. *PLoS One* 9, 1–12. <https://doi.org/10.1371/journal.pone.0086391>.
- Matt, G.E., Quintana, P.J.E., Destailats, H., Gundel, L.A., Sleiman, M., Singer, B.C., Jacob, P., Benowitz, N., Winickoff, J.P., Rehan, V., Talbot, P., Schick, S., Samet, J., Wang, Y., Hang, B., Martins-Green, M., Pankow, J.F., Hovell, M.F., 2011. Thirdhand Tobacco Smoke: Emerging Evidence and Arguments for a Multidisciplinary Research Agenda. *Environ. Health Perspect.* 119, 1218–1226. <https://doi.org/10.1289/ehp.1103500>.
- Michel, V., Yuan, Z., Ramsubir, S., Bakovic, M., 2006. Choline transport for phospholipid synthesis. *Exp. Biol. Med.* (Maywood). 231, 490–504. <https://doi.org/10.3181/07395490490> [pii].
- Müller, D.C., Degen, C., Scherer, G., Jahreis, G., Niessner, R., Scherer, M., 2014. Metabolomics using GC-TOF-MS followed by subsequent GC-FID and HILIC-MS/MS analysis revealed significantly altered fatty acid and phospholipid species profiles in plasma of smokers. *J. Chromatogr. B Anal. Technol. Biomed. Life Sci.* <https://doi.org/10.1016/j.jchromb.2014.02.044>.
- PeiYi, L., YanYan, X., YuHan, T., Min, D., Xiao, Y., Jian, S., Lin, X., Meian, H., Sheng, W., Jing, Y., YouJie, W., Yuan, L., TangChun, W., XiaoPing, M., Ping, Y., Liu, P., Xu, Y., Tang, Y., Du, M., Yu, X., Sun, J., Xiao, L., He, M., Wei, S., Yuan, J., Wang, Y., Liang, Y., Wu, T., Miao, X., Yao, P., 2017. Independent and joint effects of moderate alcohol consumption and smoking on the risks of non-alcoholic fatty liver disease in elderly Chinese men. *PLoS One* 12, e0181497. <https://doi.org/10.1371/journal.pone.0181497>.
- Pi, J., Wu, X., Feng, Y., 2016. Fragmentation patterns of five types of phospholipids by ultra-high-performance liquid chromatography electrospray ionization quadrupole time-of-flight tandem mass spectrometry. *Anal. Methods.* <https://doi.org/10.1039/C5AY00776C>.
- Pirola, C.J., Sookoian, S., 2018. Multiomics biomarkers for the prediction of nonalcoholic fatty liver disease severity. *World J. Gastroenterol.* 24, 1601–1615. <https://doi.org/10.3748/wjg.v24.i15.1601>.
- Pytel, S., Zschörnig, K., Nimptsch, A., Paasch, U., Schiller, J., 2012. Enhanced lysophosphatidylcholine and sphingomyelin contents are characteristic of spermatozoa from obese men - A MALDI mass spectrometric study. *Chem. Phys. Lipids* 165, 861–865. <https://doi.org/10.1016/j.chemphyslip.2012.11.001>.
- Råföls, P., Heijs, B., del Castillo, E., Yanes, O., McDonnell, L.A., Brezmes, J., Pérez-Taboada, I., Vallejo, M., García-Altres, M., Correig, X., 2020. rMSPROC: An R package for mass spectrometry imaging data processing. *Bioinformatics.* <https://doi.org/10.1093/bioinformatics/btaa142>.
- Råföls, P., Torres, S., Ramírez, N., Del Castillo, E., Yanes, O., Brezmes, J., Correig, X., 2017. RMSI: An R package for MS imaging data handling and visualization. *Bioinformatics* 33, 2427–2428. <https://doi.org/10.1093/bioinformatics/btx182>.
- Råföls, P., Vilalta, D., Torres, S., Calavia, R., Heijs, B., McDonnell, L.A., Brezmes, J., del Castillo, E., Yanes, O., Ramírez, N., Correig, X., 2018. Assessing the potential of sputtered gold nanolayers in mass spectrometry imaging for metabolomics applications. *PLoS One* 13, e0208908. <https://doi.org/10.1371/journal.pone.0208908>.
- Rein-Fischboeck, L., Haberl, E.M., Pohl, R., Schmid, V., Feder, S., Krautbauer, S., Liebisch, G., Buechler, C., 2018. Alpha-syntrophin null mice are protected from non-alcoholic steatohepatitis in the methionine-choline-deficient diet model but not the atherogenic diet model. *Biochim Biophys. Acta - Mol. Cell Biol. Lipids* 1863, 526–537. <https://doi.org/10.1016/j.bbalip.2018.02.006>.
- Reis, A., Spickett, C.M., 2012. Chemistry of phospholipid oxidation. *Biochim. Biophys. Acta - Biomembr.* 1818, 2374–2387. <https://doi.org/10.1016/j.bbamem.2012.02.002>.
- Schymanski, E.L., Jeon, J., Gulde, R., Fenner, K., Ruff, M., Singer, H.P., Hollender, J., 2014. Identifying small molecules via high resolution mass spectrometry: Communicating confidence. *Environ. Sci. Technol.* 48, 2097–2098. <https://doi.org/10.1021/es5002105>.
- Sherriff, J.L., Properzi, C., Oddo, J., Adams, L.A., 2016. Choline, Its Potential Role in Nonalcoholic Fatty Liver Disease, and the Case for Human and Bacterial Genes 1, 2 5–13. <https://doi.org/10.3945/an.114.007955.N>.
- Seiple, S., Apsley, A., Azmina Ibrahim, T., 2015. Fine particulate matter concentrations in smoking households: just how much secondhand smoke do you breathe in if you live with a smoker who smokes indoors? *Tob. Control* (24), e205–e211. <https://doi.org/10.1136/tobaccocontrol-2014-051635>.
- Siuzdak, G., Patti, G.J., Yanes, O., 2012. Innovation: Metabolomics: the apogee of the omics trilogy. *Nat. Rev. Mol. Cell Biol.* 13, 263–269.
- Sleiman, M., Gundel, L.A., Pankow, J.F., Jacob, P., Singer, B.C., Destailats, H., 2010. Formation of carcinogens indoors by surface-mediated reactions of nicotine with nitrous acid, leading to potential thirdhand smoke hazards. *Proc. Natl. Acad. Sci.* 107, 6576–6581. <https://doi.org/10.1073/pnas.0912820107>.
- Smith, C.A., O'Maille, G., Want, E.J., Qin, C., Trauger, S.A., Brandon, T.R., Custodio, D. E., Abagyan, R., Siuzdak, G., 2005. METLIN: a metabolite mass spectral database. *Ther. Drug Monit.* 27, 747–751.
- Smith, C.A., Want, E.J., O'Maille, G., Abagyan, R., Siuzdak, G., 2006. XCMS: Processing Mass Spectrometry Data for Metabolite Profiling Using Nonlinear Peak Alignment, Matching, and Identification. *Anal. Chem.* 78, 779–787. <https://doi.org/10.1021/ac051437y>.
- Sun, L., Liang, L., Gao, X., Zhang, H., Yao, P., Hu, Y., Ma, Y., Wang, F., Jin, Q., Li, H., Li, R., Liu, Y., Hu, F.B., Zeng, R., Lin, X., Wu, J., 2016. Early prediction of developing type 2 diabetes by plasma acylcarnitines: A population-based study. *Diab. Care* 39, 1563–1570. <https://doi.org/10.2337/dc16-0232>.
- Torres, S., Merino, C., Paton, B., Correig, X., Ramírez, N., 2018. Biomarkers of exposure to secondhand and thirdhand Tobacco smoke: Recent advances and future perspectives. *Int. J. Environ. Res. Public Health.* <https://doi.org/10.3390/ijerph15122693>.
- Vinaixa, M., Miguel, A., Rull, A., Joven, J., Correig, X., 2010. Metabolomic Assessment of the Effect of Dietary Cholesterol in the Progressive Development of Fatty Liver Disease research articles 2527–2538.
- Wishart, D.S., Jewison, T., Guo, A.C., Wilson, M., Knox, C., Liu, Y., Djoumbou, Y., Mandal, R., Aziat, F., Dong, E., Bouatra, S., Sinelnikov, I., Arndt, D., Xia, J., Liu, P., Yallou, F., Bjorn Dahl, T., Perez-Pineiro, R., Eisner, R., Allen, F., Neveu, V.,

- Greiner, R., Scalbert, A., 2012. HMDB 3.0—The Human Metabolome Database in 2013. *Nucl. Acids Res.* 41, D801–D807. <https://doi.org/10.1093/nar/gks1065>.
- Wu, G., Fang, Y.-Z., Yang, S., Lupton, J.R., Turner, N.D., 2004. Glutathione Metabolism and Its Implications for Health. *J. Nutr.* <https://doi.org/10.1093/jn/134.3.489>.
- Yuan, H., Shyy, J.Y.J., Martins-Green, M., 2009. Second-hand smoke stimulates lipid accumulation in the liver by modulating AMPK and SREBP-1. *J. Hepatol.* 51, 535–547. <https://doi.org/10.1016/j.jhep.2009.03.026>.